Unobtrusive Multimodal Monitoring of Physiological Signals for Driver State Analysis

Published Version:
Amidei, A., Rapa, P.M., Tagliavini, G., Rabbeni, R., Benini, L., Pavan, P., et al. (2025). Unobtrusive Multimodal Monitoring of Physiological Signals for Driver State Analysis. IEEE SENSORS JOURNAL, 25(5), 7809-7818 [10.1109/jsen.2024.3385480].

Availability:
This version is available at: https://hdl.handle.net/11585/1004848 since: 2025-02-12

Published:
DOI: http://doi.org/10.1109/jsen.2024.3385480

Unobtrusive Multimodal Monitoring of Physiological Signals for Driver State Analysis

Andrea Amidei*, *Graduate Member, IEEE*, Pierangelo Maria Rapa, *Graduate Member, IEEE*, Giuseppe Tagliavini, *Member, IEEE*, Roberto Rabbeni, Luca Benini, *Fellow, IEEE*, Paolo Pavan, *Senior, IEEE*, Simone Benatti, *Member, IEEE*

***Abstract*—This research introduces the second version of ANGELS, an embedded system designed to analyze PPG and EDA signals in the context of driver monitoring. ANGELS is a cost-effective and energy-efficient solution that performs real-time acquisition and processing of PPG and EDA signals, enabling continuous monitoring of driver physiological parameters. Notably, ANGELS operates autonomously without needing accelerometer data to mitigate distortions caused by vehicle motion. Following an initial validation in collaboration with Maserati, supplementary experiments were conducted within our laboratory-level driving simulator. ANGELS v2 integrates an additional EDA sensor compared to its predecessor. Despite its unobtrusive nature, ANGELS v2 features a mean absolute error of 1.19 BPM in heart rate detection and 1.9 misdetected peaks per minute in EDA peak detection, which is the standard metric to evaluate EDA. These results are achieved within a power envelope of 230 mW. These results underscore the reliability and promising potential of ANGELS v2 to enhance driver safety.**

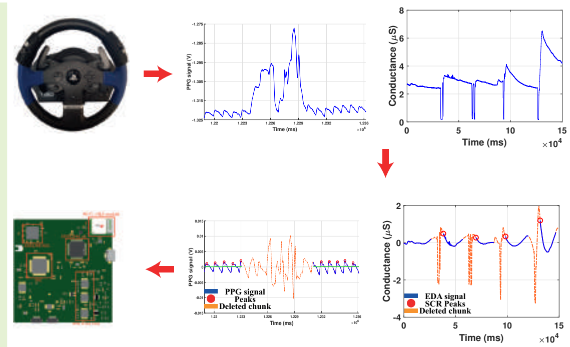

***Index Terms*—ADAS, Artifacts removal, Driver monitoring, Driver safety, Drowsiness, Electrodermal Activity, Embedded system, Human-Machine Interfaces, Low power, Photoplethysmography, Physiological signals.**

I. INTRODUCTION

Human-Machine Interaction (HMI) is gaining a remarkable traction in the automotive industry due to its potential to enhance the driving experience and improve driver safety by mitigating attention deficits and drowsiness - significant contributors to vehicle accidents. Upscale vehicles now offer a range of solutions aimed at reducing these issues.

Among commercially available solutions, most include lane assistance, collision avoidance radars, lidars, braking assistance, and cruise control [1]. In addition, several high-end vehicles incorporate driver monitoring systems to reduce accidents caused by driver drowsiness. These systems analyze steering wheel movements and behavioral features such as eye blinks or head movements through integrated cameras [2]–[9]. Fundamentally, these systems are based on a safety paradigm that evaluates vehicle behavior in unsafe situations. Their main advantages are unobtrusiveness and ease of installation within the vehicle interior.

Nevertheless, these systems lack the inherent capacity to directly asses the driver's physiological state. Monitoring specific physiological parameters provides an opportunity to gain fundamental insights into a driver's state [10]. This approach enables the implementation of predictive measures that proactively avoid unsafe scenarios, in contrast to an exclusive reliance on reactive responses based on the vehicle's behavior [11], [12]. Recent research shows that monitoring physiological signals through wearable or in-vehicle sensors allows the monitoring of driver conditions. Methods that have been extensively studied include the analysis of ECG, PPG, EDA, and EEG signals [13]. Despite their unobtrusiveness, it is noteworthy that camera-based systems are hampered by variations in lighting conditions and line-of-sight obstructions,

Submitted on 21-10-2023.

This manuscript is submitted as an extension of the conference paper A. Amidei et al., "ANGELS - smArt steeriNG wheEL for driver Safety" in 2023 9th International Workshop on Advances in Sensors and Interfaces (IWASI), 2023, pp. 15-20. IEEE Xplore URL: https://ieeexplore.ieee.org/document / 10164505. DOI: 10.1109/IWASI58316.2023.10164505.

*Corresponding author.

A. Amidei, P. Pavan, and S. Benatti are with the Department of Engineering, University of Modena and Reggio Emilia, 41125 Modena, IT (e-mail: {andrea.amidei, paolo.pavan, simone.benatti} @unimore.it).

P. M. Rapa, and L. Benini are with the Department of Electrical, Electronic, and Information Engineering, University of Bologna, 40136 Bologna, IT (e-mail: {pierangelomaria.rapa, luca.benini} @unibo.it).

G. Tagliavini, is with the Department of Computer Science And Engineering, University of Bologna, 40136 Bologna, IT (e-mail: giuseppe.tagliavini@unibo.it).

R. Rabbeni is with the Maserati Company, 41126 Modena, IT(e-mail: roberto.rabbeni@maserati.com).

L. Benini is also with the Integrated Systems Laboratory, Department of Information Technology and Electrical Engineering, ETH Zurich, 8092 Zurich, CH (e-mail: lbenini@iis.ee.ethz.ch).

This research was partially funded by the National Funded Programme 2014-2020 under grant agreement n. 1733, (ADAS+ Project). This research was partially funded by the National Funded Programme 2. This research was supported by the ETH Zurich's Future Computing Laboratory, funded by a donation from Huawei Technologies.

such as eyeglasses or sunglasses, which may affect their performance.

From a clinical standpoint, direct measures of sleep and wake states are performed by Electroencephalography (EEG) [14] analysis due to its ability to detect autonomic nervous system (ANS) activity. However, the electrode placement needed on the skin and scalp makes EEG unfeasible for unobtrusive use in an automotive context. As a result, indirect measures are becoming increasingly important to detect changes in physiological parameters indicative of driver's state alterations, such as drowsiness. Electrocardiography (ECG) [15], Photoplethysmography (PPG) [16], and Electrodermal Activity (EDA) [17] signals provide indirect insight into ANS-related states [18].

Although the ECG is widely used in research to monitor driver status, its requirement for simultaneous contact of two active electrodes plus a third reference makes it unsuitable for in-vehicle monitoring. In contrast, PPG and EDA require simpler contact interfaces. PPG is detected by a photodiode-led pair that can also be placed under one of the 2 hands holding the steering, whereas EDA needs 2 nearby electrodes that can also be placed against the palm of a hand. PPG uses an optical approach that measures changes in blood volume within microvascular tissues during each heartbeat, directly correlating with heart rate (HR) [19], while EDA reflects variations in skin electrical conductivity [20]. EDA is measured as the voltage between two electrodes subjected to a small current. EDA includes a DC component, namely the Skin Conductance Level (SCL) component, and distinct short waveforms representing the variable aspect of the signal, namely the Skin Conductance Response (SCR) component. This metric is important because it quantifies responses to internal and external stimuli [21].

Variations in sensor-skin contact can compromise the reliability of PPG and EDA signals. A common strategy to address this concern involves embedding sensor data with accelerometer data to identify signal noise associated with rapid motion. This approach is widely used in wearable devices such as wristbands and smartwatches, as validated by Burrello et al. [22].

However, approaches used in wearable devices rely on correlation and proportionality between the noise of EDA and PPG signals and measured acceleration values. These solutions do not work on the steering wheel of a car since here the main causes of noise and low signal quality are variations in contact pressure or relative hand movements with respect to the steering wheel, which are not directly measurable with an Inertial Measurement Unit (IMU).

This study presents an extended and improved version of ANGELS (smArt steeriNG wheel for driver Safety) [23], a low-cost embedded system designed for seamless integration into a vehicle steering wheel. The updated platform is customized for acquiring and processing PPG and EDA signals, enabling real-time monitoring of HR and SCR peaks without relying on accelerometer data for signal processing. The system includes a sensitive photodiode sensor unit developed by ST Microelectronics [24] and a pair of flexible AgCl electrodes (Soft-Pulse™, Dätwyler Schweiz AG) [1]. These components can be easily integrated into the steering wheel, along with a miniaturized embedded platform for real-time signal processing using a modified version of the Pan-Tompkins algorithm [25] and a custom SCR peak extraction and detection algorithm. Notably, the system is unobtrusive, features a low power consumption profile, and is economically viable, with costs in the hundreds of dollars. This design makes ANGELS a viable option for integration into a wide range of vehicles, contributing significantly to improvements in driving safety.

The main contributions of the work are:

- A novel version of ANGELS that can acquire and process continuously PPG and EDA signals from the driver in a non-invasive way.
- An improved algorithm for PPG and EDA signal analysis. We tested the algorithm on a dataset collected in the Maserati driving simulator on seven subjects and in our laboratory at the University of Modena and Reggio Emilia, where 27 subjects were involved. Our PPG peak detection algorithm achieves 99.8% Accuracy, 97.1% Sensitivity, and 99.06% Positive Predictive Value (PPV). Regarding HR detection, the Mean Absolute Error (MAE) is 1.19 BPM. About EDA, the MAE is 1,19 peak misdetected per minute. Considering both signals, the developed artifacts removal algorithm has a 92% Accuracy score, 92% Sensitivity, and 85% PPV.
- The power profiling of the system, which operates with a latency of 10 s and featuring 230 mW of power consumption.

II. Related Works

In the context of driver monitoring, combining different sensors to monitor several physiological signals stands out as a strategy to improve the accuracy and reliability of detection systems. This section explores combinations of sensors such as ECG, PPG, Electromyography (EMG), and respiratory rate (RR), each providing complementary data to provide a comprehensive picture of the driver's status.

Table I lists recent studies using physiological signals to analyze driver states. Budak et al. [26] employ a headband to collect EEG data from the driver. In contrast, Jiao et al. [27] design an integrated device for obtaining EEG and Electrooculography (EOG) signals through body-attached electrodes. As previously discussed, EEG is the gold standard for directly monitoring brain activity. Despite the less intrusive nature of wearable EEG headbands and EOG glasses, challenges arise in maintaining signal quality among driving-related movements, making them impractical for automotive applications.

Fujiwara et al. [19] and Yuda et al. [31] employ a system based on ECG and RR monitoring sensors. The correlation between Heart Rate Variability (HRV) derived from ECG and breathing patterns from RR can identify the onset of fatigue earlier than using each signal separately. While RR can be measured contactless with wearables, ECG needs hand contact.

[1]https://datwyler.com/de/unternehmen/innovation/softpulse

TABLE I
STATE OF ART COMPARISON

Authors	Signals	Acquisition	Obtrusive
Budak[26]	EEG	Wearable	Yes
Lee[28]	ECG, PPG	Wearable	Yes
Fujiwara[19]	HRV	Body attached sensors	Yes
Guede-Fernandez[29]	RR	Body attached sensors	Yes
Koh[30]	PPG	Body attached sensors	Yes
Yuda[31]	ECG, RR	Body attached sensors	Yes
Muralidharan[32]	PPG	Wearable	Yes
Jiao[27]	EEG, EOG	Body attached sensors	Yes
Sahayadhas[33]	ECG, EMG	Body attached sensors	Yes
Our Work	**PPG, EDA**	**Steering Wheel Integrated Sensors**	**No**

Similarly, Sahayadha et al. [33] combine ECG and EMG signals for driver monitoring. EMG, measuring the electrical activity of muscles, provides insights into driver movements and aids in predicting driver behavior. This work used medical-grade devices to acquire ECG and EMG signals, where EMG was explicitly employed to analyze muscle fatigue and improve ECG-based driver assessment. Like ECG, EMG needs a series of electrodes in close contact with the body, making it susceptible to electrode displacement and impractical for automotive applications.

Guede-Fernandez et al. [29] and Koh et al. [30] propose a study based on PPG and RR signals for monitoring heart activity. PPG sensors offer a less intrusive method for monitoring fatigue when used alongside devices measuring respiration rates. Lee [28] and Muralidharan [32] base their studies on a combination of ECG and PPG. The integration of ECG and PPG sensors presents an alternative approach to monitoring HRV, reducing the limitations inherent in each method when utilized independently, such as ECG's susceptibility to electrode displacement and PPG's sensitivity to motion artifacts. However, the aforementioned papers rely on body-worn sensors, which can achieve high-quality signals but are impractical in automotive applications where it is necessary that all hardware is integrated into the vehicle dashboard.

Our study introduces a novel fusion of PPG and EDA techniques. EDA sensors provide valuable ANS information, enabling stress and emotional state monitoring. Like ECG, EDA is susceptible to distortion from motion artifacts, but its acquisition at the same site, such as the hand, presents advantages. Combined with PPG, our approach enables the comprehensive evaluation of the driver's state, due mainly to the fact that noise is eliminated using a PPG-based algorithm that does not require the presence of inertial sensors

III. MATERIALS & METHODS

A. System Description

The system described in this manuscript represents an advancement of ANGELS, incorporating two primary components: (i) a sensorized steering wheel integrating PPG and EDA sensor probes and (ii) a compact board for signal acquisition and processing (refer to Fig 1). PPG probes and EDA electrodes are seamlessly integrated into the steering wheel by modifying a commercial leather steering wheel cover.

The PPG sensor probes include compact optical systems designed explicitly for PPG acquisition. These probes integrate a Silicon Photomultiplier (SiPM) photodetector coupled with infrared and red LEDs as optical light sources. The SiPM detector, developed by STMicroelectronics, features a total area of $4 \times 4\ mm^2$ with 4871 microcells arranged in a square pattern, each having a pitch of $60\mu m$ [24]. The EDA dry electrodes are made of a conductive elastomer and manufactured by Datwyler.

Both the PPG probes and EDA electrodes are housed within a 3D-printed support structure, and a long-pass optical filter is employed to safeguard the SiPM from external light interference. Wire-to-board connectors facilitate connectivity between the probes. The acquisition and processing board consists of four main blocks: (i) an analog front-end incorporating the probe power rail, a DAC to regulate the LED's current, and an operational amplifier to condition the EDA signal, (ii) the ADC ADS1298 for acquiring two channels of PPG and EDA signals, (iii) the STM32F4 microcontroller for onboard signal processing, and (iv) an esp32 for streaming acquired data via Bluetooth Low Energy (BLE) and WiFi (IEEE 802.11 b/g/n) protocols.

B. Data Acquisition

To assess the performance and reliability of the updated ANGELS version, three distinct measurement sessions were conducted involving 27 subjects. The sessions encompassed i) acquisitions on the fingers, ii) acquisitions on both fingers and palm and iii) acquisitions of PPG and EDA signals on a given set of predefined hand movements. Each experiment was performed under similar conditions and on different days to minimize cross-test variability. In the first two tests, the EDA signal acquired by ANGELS was compared with a reference signal. The reference signal relied on a BITalino EDA front-end from PLUX Biosignals [34], linked to our board for signal synchronization. Standard Kendall^{TM} H124SG electrodes from Cardinal Health, measuring 30x24 mm and equipped with a conductive solid gel for optimal adhesion, were utilized for this acquisition, ensuring high-quality EDA monitoring. The data were sampled at 1 kHz and streamed to the PC via WiFi using the TCP protocol.

The first measurement involved five volunteers aged between 20 and 30 years. Thanks to the adhesive ring, the reference device electrodes were placed on the left hand's distal phalanx of the index and middle finger. In contrast, ANGELS dry electrodes were fixed to a stable surface to prevent unwanted movements. Testers were instructed to hold the middle phalanx of the same fingers on the dry electrodes. Each measurement lasted 2 minutes, during which testers remained quiet and comfortably seated. The Valsalva Maneuver was performed midway through the acquisition to induce a cardiovascular change and stimulate the sympathetic nervous system, producing an SCR event [35]. The Valsalva maneuver

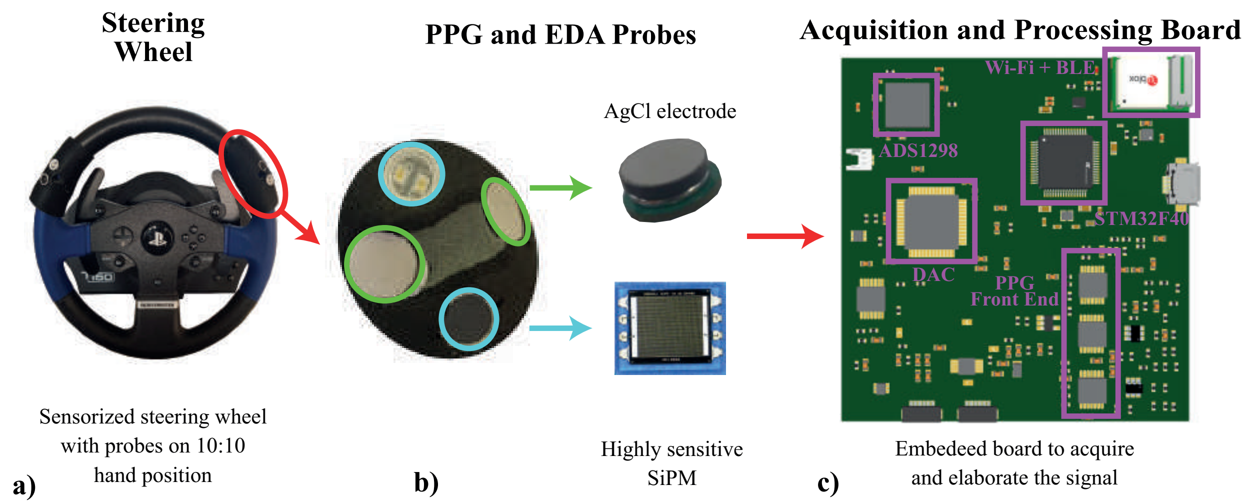

Fig. 1. Block scheme of the proposed system, which comprises three main blocks: a) a steering wheel as a base platform for placing sensor probes and allowing continuous signal acquisition; b) two pairs of PPG and EDA probes, which are placed close together to ensure the acquisition of both signals on the same site, and they are encapsulated into a steering wheel cover to gather driver physiological signals from the palm without causing discomfort; c) an acquisition and processing board where the main components are highlighted in purple. There are ADS1298 to make the AD signals conversion, Wi-Fi and Bluetooth module, DAC to control the LEDs current, PPG front-end to polarize the photodetectors, and an STM32F40 for online data elaboration. The board also includes a conditioning circuit for EDA signals.

consists of forced expiration against a closed glottis. It causes a cardiovascular change that stimulates the sympathetic nervous system and thus produces an SCR event [35]. This experiment aimed to assess the similarity between signals acquired by our device and the reference in the same site.

The second measurement involved twelve testers between 20 and 30 years of age. As in the first protocol, the reference device electrodes were placed on the index and medium finger of the left hand. Our device was inserted into a steering wheel of the University of Modena and Reggio Emilia driving simulator to simulate in-car acquisition. The protocol followed the method used during the first experiment, with testers seated steadily in the simulator. This experiment aimed to compare the hand-acquired EDA signal with the one acquired at the reference site and assess its quality. A total of 24 minutes of signals were recorded.

The third measurement involved ten volunteers between 20 and 30 years of age, distinct from those in the second experiment. PPG and EDA signals were acquired simultaneously with sensors integrated into the steering wheel, as shown in Fig. 1.b. Testers were instructed to keep the left hand steady for 5 minutes to ensure robust signal acquisition. Controlled movements were introduced every 30 seconds to induce artifacts, including removing hands, sliding the hand, and making rapid left and right steering wheel movements. This experiment aimed to create controlled artifacts on PPG and EDA signals and evaluate the performance of the artifact removal algorithm outlined in section III-C. In total, 50 minutes of PPG and EDA signals were recorded. Across all experiments, a cumulative duration of 84 minutes of signals was acquired.

C. Algorithm description

One of the main advances of ANGELS is a novel algorithmic approach to elaborate the acquired PPG and EDA signals. This is a robust time-domain algorithm composed of two parts: i) a PPG peaks detection block described in [23], and ii) an EDA peaks detection block.

1) PPG peak detection: The PPG processing algorithm comprises three main stages: a filtering stage, an artifact removal block, and a peak detection stage [23]. Distortions due to driving movements affect signals acquired on the steering wheel, so proper artifact removal is paramount. Following band-pass filtering between 0.5 and 10 Hz, a rolling standard deviation is applied to assess the signal quality and identify windows affected by motion artifacts, as depicted by the *Artifacts Removal* block in Fig. 2c). The rolling standard deviation is computed for each sample within a 1 s time window, moving one sample at a time. If the standard deviation overcomes a threshold set at 0.005, a 5 s window (2.5 s backward, 2.5 s forward) is removed [23]. Through a tuning phase, it was empirically determined that this threshold exhibited optimal performance in correctly discriminating corrupted PPG windows from intact ones in the dataset acquired in [16]. Fig. 2 provides an example of the algorithm's functioning and block scheme, and Fig. 2b) represents the outcome of artifact removal on a signal segment. Due to probe proximity, as shown in Fig. 1.b, driving movements are bound to generate simultaneous artifacts on both EDA and PPG signals. When hands cover the PPG sensors only partially, also the EDA electrodes remain exposed, leading to artifacts in both signals. To mitigate this effect, a 5-second window was removed when an artifact was detected.

After the artifact removal phase, precise peak detection is ensured by a Pan-Thompkin-like algorithm, which integrates adaptive thresholding to detect HR frequency. Peak detection is detailed in the Algorithm 1 diagram, where the starting derivation and integration phases of the original Pam-Tompkins algorithm is substituted with the zeroing of the PPG negative value. As shown in Algorithm 1 diagram, the algorithm is based on a while loop that iterates over 50s long signal windows, with a 40s overlap. After refreshing PPG data using the Shift data_buffer routine, the Searchback condition is evaluated. If the interval between the current sample and the last peak exceeds a predefined boundary (BS), indicating a peak misidentification, the algorithm initiates a search for a peak within the range delimited by the current sample and previous peaks. If the Searchback condition is not met, the algorithm continues with peak detection. From line 32, an adaptive thresholding approach is deployed. This method calculates the median peak interval for each 10-second period based on the preceding 13 detected peaks. Should this interval fall below the current minimum distance (min_dist) plus $0.2 \times fs$ for eight consecutive times, the threshold is reduced by 0.01. Conversely, if it surpasses the same criterion for eight consecutive iterations, augmentation by $0.01 \times fs$ ensues. Consequently, min_dist adapts with the

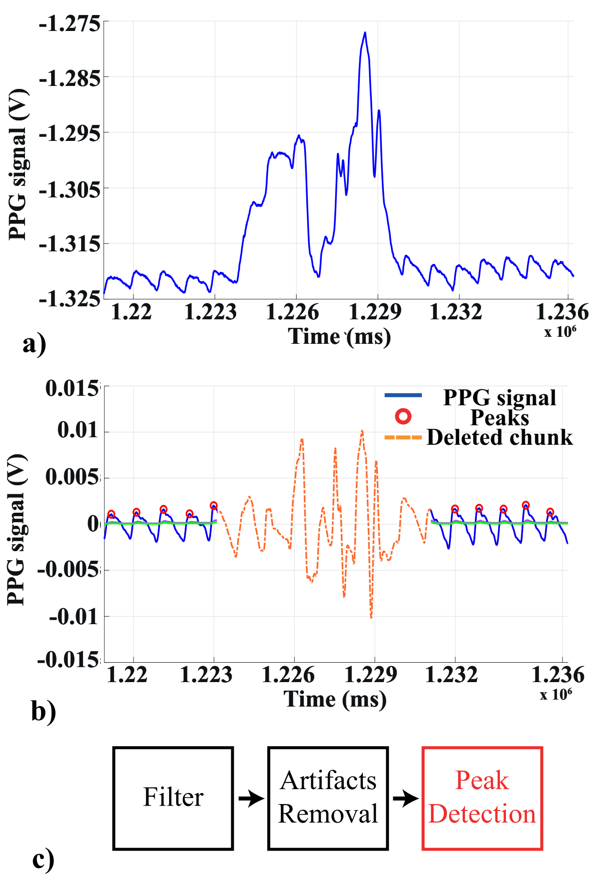

Fig. 2. Block diagram of the algorithm used to detect PPG peaks, along with an instance of the ANGELS elaboration pipeline for a signal window. Figure a) displays a window of the raw PPG signal, while figure b) shows the same window with the processed signal. The blue line represents the PPG signal, and the orange dotted line depicts the removed corrupted portion of the signal, with red circles indicating the identified peaks. Figure c) offers a block diagram of the algorithm, outlining its key stages [23].

peak-to-peaktrend, thereby recalibrating thresholds in the peak detection process every 10 seconds. This adaptive paradigm enhances algorithmic reliability, as demonstrated by [23].

Algorithm 1 Peak Detection Stage

1: **Input:** $PPG\ Signal$
2: **Ouput:** $PPG\ Peaks$
3: $PPG(PPG < 0) \leftarrow 0$, $s \leftarrow 1$, $BS \leftarrow 1.6 \times fs$
4: **while** $s <$ length(PPG) **do**
5: Shift data_buffer
6: $current \leftarrow \max(BS, s)$
7: **if** Searchback condition is met **then**
8: **for** $i \leftarrow 1$ to $current$ **do**
9: $peaki \leftarrow data\_buff(i)$
10: **if** $peaki > threshold2$ **then**
11: **if** no peak **or**$(s - BS + i) - Prev\_Peak \geq min\_dist)$ **then**
12: $spki \leftarrow 0.875 \times spki + 0.125 \times peaki$
13: $New\_Peak \leftarrow s - BS + i$
14: **else if** $data\_buff(s - BS + i) < peaki$ **then**
15: $Prev\_Peak \leftarrow s - BS + i$
16: **else**
17: $npki \leftarrow 0.875 \times npki + 0.125 \times peaki$
18: $threshold1 \leftarrow npki + 0.25 \times (spki - npki)$
19: $threshold2 \leftarrow 0.5 \times threshold1$
20: **else**
21: $peaki \leftarrow data\_buff(current)$
22: **if** $peaki > threshold1$ **then**
23: $spki \leftarrow 0.875 \times spki + 0.125 \times peaki$
24: **if** no peak **or** $s - Prev\_Peak \geq min\_dist$ **then**
25: $New\_Peak \leftarrow s$
26: **else if** $data\_buff(current - s + Prev\_Peak) < peaki$ **then**
27: $Prev\_Peak \leftarrow s$
28: **else**
29: $npki \leftarrow 0.8 \times npki + 0.2 \times peaki$
30: Update threshold1 and threshold2
31: Every 10 seconds
32: **while** $m <$ (length$(Peaks) - 13)$ **do**
33: **for** $t \leftarrow 1$ to 8 **do**
34: $peaks\_dist \leftarrow Peaks(m + t) - Peaks(m + t - 1)$
35: **if** mean$(peaks_dist) < min_dist + (0.2 \times fs)$ **then**
36: $count\_1 \leftarrow count\_1 + 1$
37: **if** $count\_1 > 8$ **then**
38: $min\_dist \leftarrow min\_dist - (0.01 \times fs)$
39: $count\_1, count\_2 \leftarrow 0$
40: **else**
41: $count\_2 \leftarrow count\_2 + 1$
42: **if** $count\_2 > 8$ **then**
43: $min\_dist \leftarrow min\_dist + (0.01 \times fs)$
44: $count\_1, count\_2 \leftarrow 0$

2) EDA peak detection: The EDA processing algorithm encompasses four key blocks: a filtering stage, an artifact removal block, the signal division into SCR and SCL components, and an SCR peaks detection block. Fig. 3 illustrates the algorithm's block diagram and an example of signal window elaboration. Following a second-order low-pass filtering at 2 Hz, the artifact removal block is applied, as detailed in the previous section III-C.1. The SCR and SCL components are isolated using a 0.5 Hz fifth-order low-pass filter and a fifth-order high-pass filter at 0.5 Hz.

We employed an algorithm based on the approach developed by Kim et al. [36] to detect SCR occurrences, namely the SCR peaks, showed in Algorithm 2. The algorithm works on signal segments of 50 seconds in a while loop. SCR peaks are identified by locating two consecutive zero crossings, from negative to positive and positive to negative. The first for cycle, line 5, serves to find the first zero crossing point. The second for, line 8, determines the consecutive point. The peak amplitude is determined by finding the maximum value between these two zero crossings. Subsequently, SCR peaks with an amplitude less than 10% of the maximum SCR amplitude in the considered segment are excluded, following the procedure outlined in [36]. The threshold is calculated on the 50-second segment at the first iteration; afterward, it is updated considering only the new 10-second signal. This procedure allows us to consider contextual information about the level of SCR amplitude for the signal under investigation, which can vary considerably. This approach offers an advantage over conventional SCR detection by human visual inspection, where the threshold level is set arbitrarily, making objective analysis complex [36]. Notably, this method eliminates the need for an explicitly set threshold, a significant advantage given the inherent variability in EDA signal values across individuals and the unconventional acquisition method employed in our study, further contributing to increased signal variability.

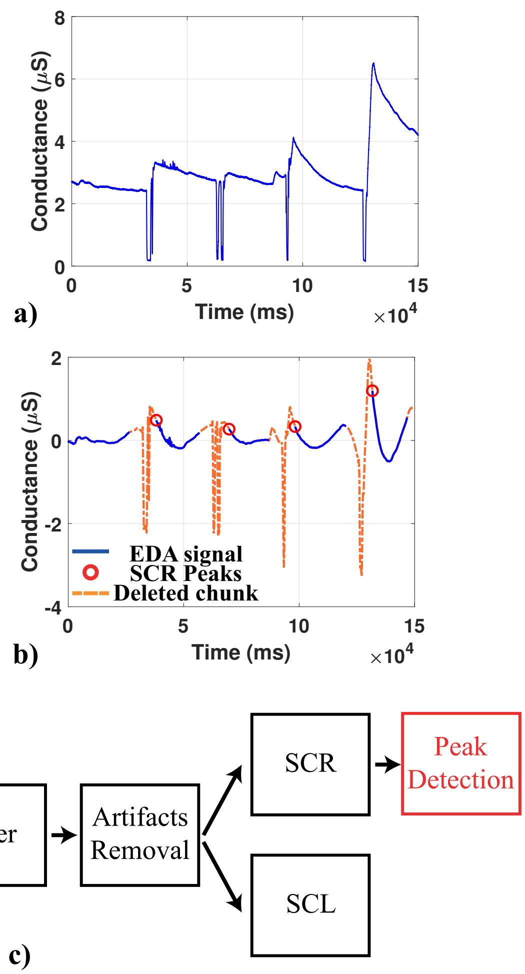

Fig. 3. Block diagram of the EDA elaboration algorithm and an example of the ANGELS elaboration pipeline for a signal window. In part a), a segment of unprocessed EDA data is shown. In part b), the SCR component is shown in the same window after the algorithm has been processed: the blue line represents the SCR signal, the orange dotted line reflects the removed corrupted portion of the signal, and the red circles indicate the detected peaks. In c), a block diagram of the algorithm is shown, outlining its main steps.

Algorithm 2 SCR Peak Detection Stage

1: **Input:** $SCR\ component$
2: **Output:** $SCR\ Peaks$
3: $thr \leftarrow \max(signal)/10$
4: **while** $i < \text{length}(signal)$ **do**
5: **for** $i < \text{length}(signal)$ **and** $start = 0$ **do**
6: **if** $(signal[i] \times signal[i-1]) < 0$ **then**
7: $start \leftarrow i - 1$
8: **for** $i < \text{length}(signal)$ **do**
9: **if** $(signal[i] \times signal[i-1]) < 0$ **then**
10: $stop \leftarrow i - 1$
11: $segment \leftarrow \text{signal}[start : stop]$
12: **if** $(\max(segment) > 0)$ **and** $(\max(segment) > thr)$ **and** $(start \times stop \neq 0)$ **then**
13: $peak \leftarrow \text{find\_max}(segment) + start$
14: $start \leftarrow stop$
15: $stop \leftarrow 0$

IV. Experimental Results

In this section, we evaluate the performance of the latest ANGELS release, focusing on validating the acquired EDA signals. Our analysis includes key metrics such as correlation index, absolute error, accuracy, and power consumption.

Initially, a comparative analysis was conducted between the EDA-acquired signal and the EDA reference to determine their level of similarity. The primary objective was to evaluate the signals' similarity by calculating their Pearson correlation coefficient. This coefficient measures the linear correlation between two datasets, and it is determined by the ratio of the covariance of two variables to the product of their standard deviations. The resulting numerical value falls within the range of -1 to 1. A value of -1 indicates no correlation, while 1 signifies a high degree of similarity between the signals. Notably, we based this assessment on data from the first experiment, where the EDA signals were acquired simultaneously and at the same location. The dataset analysis revealed a remarkable average correlation coefficient of 0.84 among the acquired signals. As a result, the signals recorded by our system closely match the reference signal, which aligns with our expectations. Furthermore, these results validate the

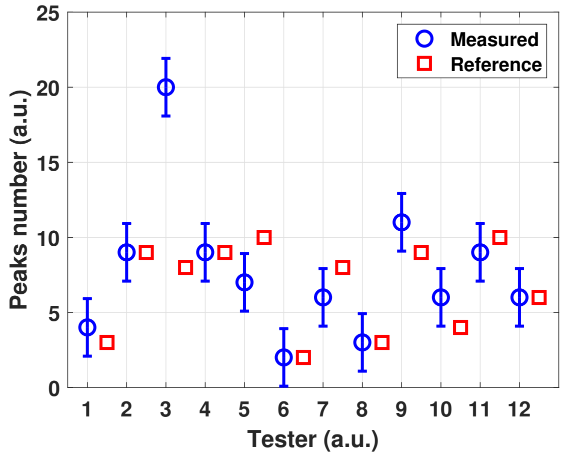

Fig. 4. Box plot displaying the number of peaks detected in the acquired signals, represented by blue circles according to our system, while the blue line shows the error bars depicting the MAE. Additionally, the red squares indicate the number of peaks detected in the reference signals.

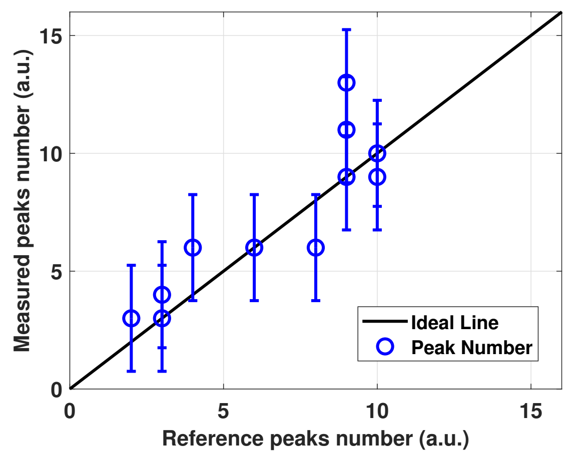

Fig. 5. Comparison of the number of peaks, expressed in a. u., from the reference signal (horizontal axis) and the number of peaks estimated by ANGELS (vertical axis). The blue circles are the points, the blue lines are the error bars depicting the MAE, and the black line is the bisector representing the ideal position of the points.

effectiveness of the implemented dry electrodes, which are more feasible than the wet ones.

Considering the second experiment, the evaluation focuses on signal similarity by analyzing peak occurrences within the SCR component. We employed this approach instead of studying the correlation coefficient, mainly due to variations in the measurement location compared to the previous experiment. Additionally, the SCR peak number within a predefined time interval is one of the most informative metrics for EDA analysis, making it a more appropriate evaluation feature for our context. In this regard, we calculate the peak number within a specified time frame, precisely 1 minute of signal starting from the midway to the end of the acquisition. This interval ensures the collection of signals during and after the Valsalva Maneuver, thereby accounting for peaks induced by the intended stimulus while excluding peaks resulting from uncontrolled stimuli. The same methodology is applied to the reference signal. Subsequently, the mean absolute error (MAE) is employed as a metric to quantify the accuracy of our peak count estimation in 1-minute time intervals. The MAE is defined as follows:

$$MAE = \frac{\sum_{i=1}^{n}(PeakN_i^{pred} - PeakN_i^{true})}{n}$$

where $PeakN^{pred}$ indicates the Peak Number detected on the palm, $PeakN^{true}$ indicates the value of peaks detected on the reference signal, and n is the number of windows.

To evaluate the algorithm performance in removing motion artifacts, we adopted three metrics: Positive Predictive Value (PPV), Sensitivity, and Accuracy.

In Fig 4, a box plot is presented to compare the number of detected peaks in the measured signal (blue circles) and the reference signal (red squares) calculated in the same interval (1 minute). The blue lines are error bars reporting the MAE. The x-axis denotes the individual testers. The comparison considers intervals, including the detected peaks along with the associated error bars. Except for testers numbered 3 and 5, all intervals enclosed the peak numbers observed in the reference signal. This discrepancy is attributed to unforeseeable factors, such as involuntary movements or variations in sweating levels between the finger and palm, capable of distorting the signal. Nevertheless, testers 3 and 5 constitute outliers within our dataset and do not exert a discernible influence on the overall results.

The scatter plot in Fig. 5 shows the correlation between the measured and reference peaks, represented by blue circles with corresponding error bars, similar to Fig. 4. The black bisector line is the theoretical alignment of points. Notably, within the intervals defined by the error bars, all data points intersect the theoretical line, validating the measurement's accuracy. The outcomes from both Fig. 4 and Fig. 5 underscore the information reliability acquired through our system. Furthermore, as previously described, the SCR peak number within a predefined time interval is considered a key feature of the EDA analysis. This metric is commonly employed in analyzing human behavior, particularly in contexts related to stress or drowsiness [37]. Consequently, these results establish ANGELS as a trustworthy and effective solution for monitoring the driver's physiological state.

The third experimental phase refers to the assessment of the artifacts removal algorithm. Fig.6 illustrates the algorithm's outcomes, presenting raw PPG and EDA signals in Fig.6 a) and b), respectively. The high and rapid peaks in the signals are the distortions induced by controlled driver movements, as described in Sec III-B. In particular, movement artifacts exhibit significantly higher absolute values concerning the useful signal, leading to strong signal corruption. In Fig. 6 c) and d), the same signals are plotted post-application of the artifacts removal block. The absent portions indicate segments deleted by the elaboration algorithm detailed in Sec III-C.

Table II resumes the filter algorithm's performance, utilizing the designated metrics for each assessed tester. However, it is noteworthy that specific drivers exhibit metric values lower than expected. This discrepancy arises because of the algorithm's inability to dynamically adjust the threshold value,

This article has been accepted for publication in IEEE Sensors Journal. This is the author's version which has not been fully edited and content may change prior to final publication. Citation information: DOI 10.1109/JSEN.2024.3385480

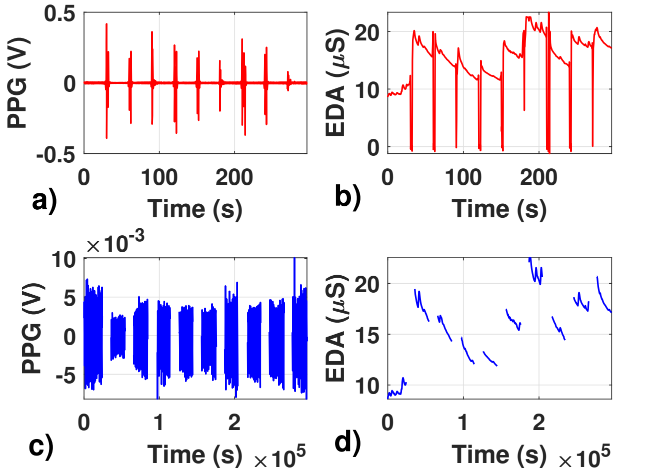

Fig. 6. Example of the artifact removal on the PPG and EDA signal simultaneously on volunteer 3. In a) and b), the raw PPG and the raw EDA signals are depicted in red. The rapid signal variations are the movement artifacts. In c) and d), the same signal windows after the PPG and EDA filtering and artifacts removal stages, respectively, are depicted in blue.

TABLE II
PPV, SENSITIVITY, AND ACCURACY OF EACH ANALYZED TESTER.

Volunteers	PPV (%)	Sensitivity (%)	Accuracy (%)
1	33.6	64.0	67.9
2	80.2	100	90.5
3	100	100	100
4	100	100	100
5	65.4	54.9	73.4
6	100	100	100
7	100	100	100
8	79.2	100	90.9
9	90.3	100	96.0
10	100	100	100

fixed at 0.005 (refer to Sec. III-C.1), which occasionally misclassifies signal segments not correlated with controlled movements. Consequently, signal segments are erroneously removed even when the driver's hand remains steady. Nonetheless, the algorithm achieves a mean PPV of 85.0 %, a mean accuracy of 92.0 %, and an overall sensitivity of approximately 92.0 %. These elevated values underscore the algorithm's efficacy in removing non-usable signal segments, particularly when contact between the steering wheel and the driver's hand is compromised.

Table I compares our approach with other SoA Biological-based driver's state detection systems. We focus our comparison on the deployability of a car cockpit; most of these systems rely on wearable devices, e.g., headbands, smartwatches, etc., and do not investigate the embeddability of the system in a real vehicle. In contrast, our solution explicitly targets a real-world scenario, considering biological signals that can be collected unobtrusively and offering algorithmic solutions compatible with a real-time domain.

Finally, we tested the proposed solution for latency and power consumption. As outlined in Section III-C, the algorithm includes two main components: PPG peak detection and

TABLE III
CYCLES, LATENCY, AND ENERGY CONSUMPTION FOR EACH BLOCK OF THE PROPOSED ALGORITHM. ALL THE RESULTS ARE COMPUTED ON A 10S WINDOW.

	Cycles (#)	Latency (ms)	Energy (mJ)
PPG filtering	250868	2.99	0.20
Artifacts removal	191000	2.27	0.15
PPG Peak detection	5120000	60.95	4.02
EDA filtering	259329	3.09	0.20
SCR Peak detection	42000	0.50	0.03

SCR peak detection. We analyzed the execution breakdown to assess system latency. As described in Sec III-C, after an initial 50-second data acquisition, the signal processing is performed only on the new 10-second signal segment. For this reason, the results illustrated in Table III refer to this time window. The cumulative latency across all blocks is 69.80 ms, notably less than the window duration. Consequently, the window duration represents the maximum latency for the system. Considering that ANGELS is mostly intended for automotive applications, this latency is acceptable because the biological parameters we want to monitor (i.e., sleepiness and stress) have a slow rate of change concerning HR and SCR variations. Regarding the power envelope of the system, starting from the measurement made in the previous work [23], we specifically evaluated the contribution of the EDA acquisition device and the algorithm for processing it. Table III shows that the data elaboration contributes 4.60 mJ. Considering the hardware components, such as the LEDs and their driver, the supply stages, and the μC, the total power consumption is 230 mW. This value is compatible with the typical constraints of automotive applications.

Table IV outlines the most relevant features of the new version of ANGELS. The experimental result demonstrates the system's reliability in defining the relevant features of the PPG and EDA signals while being unobtrusive and maintaining low latency and affordable power consumption for the automotive context.

TABLE IV
REVIEW TABLE OF THE MAIN CHARACTERISTIC OF ANGELS.

	Feature	Value
PPG	PPV	99.9 %
	Accuracy	99.9 %
	Sensitivity	97.0 %
	MAE	1,19 BPM
EDA	PPV	84.9 %
	Accuracy	91.9 %
	Sensitivity	91.9 %
	MAE	1.90 a.u.
System	Power Consumption	230 mW
	Latency	120.0 ms

V. CONCLUSION

Adopting biosignal-based HMIs has gained significant prominence within the automotive industry, primarily focusing on enhancing driving safety and driver comfort. This paper introduces an improved version of ANGELS, which is now able to acquire EDA signals and process them together with

PPG in real time, allowing the accurate detection of HR and SCR peaks. Notably, this system has been integrated into the vehicle's steering wheel, ensuring user comfort and system feasibility. Moreover, it can eliminate motion artifacts and common noise in physiological signals without needing accelerometers typically employed in wearable systems. ANGELS v2 has achieved noteworthy precision, with a heart rate detection accuracy of 1.19 BPM and an MAE of 1.9 peak number per minute in the SCR peak analysis while maintaining a conservative power consumption of 230 mW. Future research endeavors will encompass the integration and analysis of additional sensors to improve artifact removal performance, culminating in developing a robust, cost-effective system poised to meet the needs of the lower-middle market sector of the automotive industry.

Acknowledgment

A special thanks to Eng. Gianfranco Bordonaro for leading the DIL simulator setup and the night-time driving sessions together with: Eng. Beniamino Canu, Eng. Pasquale Sessa, Eng. Gabriele Maria D'Auria, Eng. Matteo Angelini, Dr. Mario D'Agostino, Eng. Enrico Maria Talarico, Eng. Dario Rezaei Riabi.

References

[1] J. Nidamanuri *et al.*, "A Progressive Review: Emerging Technologies for ADAS Driven Solutions," en, *IEEE Transactions on Intelligent Vehicles*, vol. 7, no. 2, pp. 326–341, Jun. 2022. DOI: 10.1109/TIV.2021.3122898.
[2] *Driver drowsiness detection*, en. [Online]. Available: www.bosch-mobility.com/en/solutions/assistance-systems/driver-drowsiness-detection/ (visited on 02/06/2024).
[3] *On World Sleep Day, Ford 'Sleep Suit' Delivers a Wake-Up Call on the Dangers of Driving While Drowsy — Ford of Europe — Ford Media Center*. [Online]. Available: www.media.ford.com/content/on-world-sleep-day--ford-sleep-suit-delivers-a-wake-up-call-on-t.html (visited on 02/06/2024).
[4] *Iteris Announces Introduction of Industry-First Lane Departure Warning Data Collection Product "Safety Direct & trade" for the Heavy Truck Market — Iteris, Inc.* [Online]. Available: www.iteris.com/news/iteris-announces-introduction-industry-first-lane-departure-warning-data-collection-product (visited on 02/06/2024).
[5] *No Doze: Mercedes E-Class alerts drowsy drivers*, en-US, Section: News, Dec. 2008. [Online]. Available: www.autoweek.com/news/a2032716/no-doze-mercedes-e-class-alerts-drowsy-drivers/ (visited on 02/06/2024).
[6] *EyeSight Driver Assist Technology — Subaru*, en, Section: EyeSight Driver Assist Technology — Subaru. [Online]. Available: www.subaru.com/eyesight.html (visited on 02/06/2024).
[7] *Lexus safety system+*. [Online]. Available: https://www.lexus.com/models/GX/safety/pre-collision-system (visited on 03/17/2023).
[8] *Driver alert system — Volkswagen UK*, en. [Online]. Available: www.volkswagen.co.uk/en/technology/car-safety/driver-alert-system.html (visited on 02/06/2024).
[9] *Your Volvo car will understand you when you're not at your best – and step in when you need support*, en-gb. [Online]. Available: www.media.volvocars.com/global/en-gb/media/pressreleases/304020/your-volvo-car-will-understand-you-when-youre-not-at-your-best-and-step-in-when-you-need-support (visited on 02/06/2024).
[10] M. Q. Khan and S. Lee, "A comprehensive survey of driving monitoring and assistance systems," *Sensors*, vol. 19, no. 11, 2019. DOI: 10.3390/s19112574.
[11] M. Doudou *et al.*, "Driver drowsiness measurement technologies: Current research, market solutions, and challenges," *International Journal of Intelligent Transportation Systems Research*, pp. 1–23, 2019.
[12] M. Q. Khan and S. Lee, "A Comprehensive Survey of Driving Monitoring and Assistance Systems," en, *Sensors*, vol. 19, no. 11, p. 2574, Jan. 2019, Number: 11 Publisher: Multidisciplinary Digital Publishing Institute. DOI: 10.3390/s19112574.
[13] *Various Approaches for Driver and Driving Behavior Monitoring — Proceedings of the 2013 IEEE International Conference on Computer Vision Workshops*. [Online]. Available: https://dl.acm.org/doi/abs/10.1109/ICCVW.2013.85 (visited on 11/21/2022).
[14] F. Wang *et al.*, "A Driving Fatigue Feature Detection Method Based on Multifractal Theory," en, *IEEE Sensors Journal*, vol. 22, no. 19, pp. 19 046–19 059, Oct. 2022. DOI: 10.1109/JSEN.2022.3201015.
[15] M. Sunagawa *et al.*, "Comprehensive Drowsiness Level Detection Model Combining Multimodal Information," en, *IEEE Sensors Journal*, vol. 20, no. 7, pp. 3709–3717, Apr. 2020. DOI: 10.1109/JSEN.2019.2960158.
[16] A. Amidei *et al.*, "Validating Photoplethysmography (PPG) data for driver drowsiness detection," in *2021 IEEE International Workshop on Metrology for Automotive (MetroAutomotive)*, Jul. 2021, pp. 147–151. DOI: 10.1109/MetroAutomotive50197.2021.9502865.
[17] A. Chowdhury *et al.*, "Sensor Applications and Physiological Features in Drivers' Drowsiness Detection: A Review," *IEEE Sensors Journal*, vol. 18, no. 8, pp. 3055–3067, Apr. 2018, Conference Name: IEEE Sensors Journal. DOI: 10.1109/JSEN.2018.2807245.
[18] B. Mazzoni *et al.*, "An Optimized Heart Rate Detection System Based on Low-Power Microcontroller Platforms for Biosignal Processing," en, in *Advances in System-Integrated Intelligence*, ser. Lecture Notes in Networks and Systems, Cham: Springer International Publishing, 2023, pp. 160–170. DOI: 10.1007/978-3-031-16281-7_16.
[19] K. Fujiwara *et al.*, "Heart Rate Variability-Based Driver Drowsiness Detection and Its Validation With EEG," *IEEE Transactions on Biomedical Engineering*, vol. 66, no. 6, pp. 1769–1778, Jun. 2019, Conference Name: IEEE Transactions on Biomedical Engineering. DOI: 10.1109/TBME.2018.2879346.
[20] W. Boucsein, *Electrodermal Activity*, en. Springer Science & Business Media, Feb. 2012, Google-Books-ID: 6N6rnOEZEEoC.
[21] W. Menghui *et al.*, "EDA Signal Processing Algorithms to Study the Influence of Flicker on EDA Signal," in *2022 International Conference on Electrical Engineering and Photonics (EExPolytech)*, ISSN: 2771-697X, Oct. 2022, pp. 44–47. DOI: 10.1109/EExPolytech56308.2022.9950849.
[22] A. Burrello *et al.*, "Embedding temporal convolutional networks for energy-efficient PPG-based heart rate monitoring," *ACM Transactions on Computing for Healthcare (HEALTH)*, vol. 3, no. 2, pp. 1–25, 2022.
[23] A. Amidei *et al.*, "ANGELS - Smart Steering Wheel for Driver Safety," in *2023 9th International Workshop on Advances in Sensors and Interfaces (IWASI)*, ISSN: 2836-7936, Jun. 2023, pp. 15–20.
[24] M. Mazzillo *et al.*, "Silicon Photomultiplier Technology at STMicroelectronics," en, *IEEE Transactions on Nuclear Science*, vol. 56, no. 4, pp. 2434–2442, Aug. 2009. DOI: 10.1109/TNS.2009.2024418.
[25] J. Pan and W. J. Tompkins, "A real-time QRS detection algorithm," *IEEE Transactions on Biomedical Engineering*, no. 3, pp. 230–236, 1985.
[26] U. Budak *et al.*, "An Effective Hybrid Model for EEG-Based Drowsiness Detection," *IEEE Sensors Journal*, vol. 19, no. 17, pp. 7624–7631, Sep. 2019, Conference Name: IEEE Sensors Journal.
[27] Y. Jiao *et al.*, "Driver sleepiness detection from EEG and EOG signals using GAN and LSTM networks," *Neurocomputing*, vol. 408, pp. 100–111, Sep. 2020. DOI: 10.1016/j.neucom.2019.05.108.
[28] H. Lee *et al.*, "Using Wearable ECG/PPG Sensors for Driver Drowsiness Detection Based on Distinguishable Pattern of Recurrence Plots," en, *Electronics*, vol. 8, no. 2, p. 192, Feb. 2019.
[29] F. Guede-Fernandez *et al.*, "Driver Drowsiness Detection Based on Respiratory Signal Analysis," en, *IEEE Access*, vol. 7, pp. 81 826–81 838, 2019.
[30] S. Koh *et al.*, "Driver drowsiness detection via PPG biosignals by using multimodal head support," in *2017 4th International Conference on Control, Decision and Information Technologies (CoDIT)*, Apr. 2017, pp. 0383–0388.
[31] E. Yuda *et al.*, "Changes in Respiration Pattern Preceding Drowsiness During Driving: - Ambulatory Respiration Monitoring by Smart Shirts Sensors -," en, in *International Symposium on Affective Science and Engineering*, ISSN: 2433-5428 Issue: 0 Journal Abbreviation: ISASE, vol. ISASE2020, 2020, pp. 1–2. DOI: 10.5057/isase.2020-C000018.

[32] M. J *et al.*, "Smart Safety and Accident Prevention System," en, *E3S Web of Conferences*, vol. 399, V. Vijayan and T. Senthil Kumar, Eds., p. 01 006, 2023. DOI: 10.1051/e3sconf/202339901006.

[33] A. Sahayadhas *et al.*, "Physiological signal based detection of driver hypovigilance using higher order spectra," *Expert Systems with Applications*, vol. 42, no. 22, pp. 8669–8677, Dec. 2015.

[34] *Electrodermal Activity (EDA) Sensor*, en. [Online]. Available: https://www.pluxbiosignals.com/products/electrodermal-activity-eda-sensor (visited on 10/17/2023).

[35] S. Srivastav *et al.*, "Valsalva Maneuver," eng, in *StatPearls*, Treasure Island (FL): StatPearls Publishing, 2023. [Online]. Available: http://www.ncbi.nlm.nih.gov/books/NBK537248/.

[36] K. H. Kim *et al.*, "Emotion recognition system using short-term monitoring of physiological signals," eng, *Medical & Biological Engineering & Computing*, vol. 42, no. 3, pp. 419–427, May 2004.

[37] A. Amidei *et al.*, "Driver Drowsiness Detection: A Machine Learning Approach on Skin Conductance," en, *Sensors*, vol. 23, no. 8, p. 4004, Apr. 2023.

Andrea Amidei (Graduate Student Member, IEEE) received his M.Sc. degree in Electronic Engineering from the University of Modena and Reggio Emilia, Italy, in 2020. He is currently working on his Ph.D. in Automotive Engineering for Intelligent Mobility under the supervision of Prof. P. Pavan at DIEF department University of Modena and Reggio Emilia. His research interests include the design of driver monitoring systems using biosignals to prevent dangerous behaviors during driving.

Pierangelo Maria Rapa received his M.Sc. degree in Electronic Engineering from the University of Bologna, Italy, in 2022. He is currently working on his Ph.D. in Automotive Engineering for Intelligent Mobility under the supervision of Prof. S. Benatti at DEI department, University of Bologna. His research interests include biosignals and ultra-low-power HMIs with specific emphasis on their application in the automotive industry.

Giuseppe Tagliavini (Member, IEEE) received a Ph.D. degree in Electronic Engineering and Information Technologies from the University of Bologna, Bologna, Italy, in 2017. He is currently an Assistant Professor with the Department of Computer Science and Engineering (DISI) at the University of Bologna. He has co-authored over 50 papers in international conferences and journals. His main research interests include parallel programming models for embedded systems and optimization of algorithms for biosignal analysis.

Roberto Rabbeni is responsible for HIL/DIL Systems & Innovation in the Virtual Test Properties Engineering Team at Stellantis. Dr. Rabbeni earned his Ph.D. in Energy and Information Technology and completed his undergraduate studies at the University of Palermo. His research pursuits revolve around the domains of control system theory, modeling, identification techniques, power electronics, and virtual engineering, spanning from theoretical frameworks to practical implementation. He has actively engaged in collaborative efforts with researchers across various engineering disciplines.

Luca Benini (Fellow, IEEE) holds the chair of digital Circuits and systems at ETH Zurich, Switzerland, and is a Full Professor at the Università di Bologna, Italy. He received his Ph.D. from Stanford University. Dr. Benini's research interests are energy-efficient parallel computing systems, smart sensing micro-systems, and machine learning hardware. He is a Fellow of the ACM and a member of the Academia Europaea. He is the recipient of the 2016 IEEE CAS Mac Van Valkenburg Award, the 2020 EDAA Achievement Award, the 2020 ACM/IEEE A. Richard Newton Award and the 2023 IEEE CS E.J. McCluskey Award.

Paolo Pavan (Senior, IEEE) is a Professor of Electronics at the University of Modena and Reggio Emilia, Italy. He has been the Dean of the Electronics Engineering Program and he is now the Rector's Delegate for Scientific Research. His research interests are in the characterization, modeling and optimization of non-volatile memory devices, in particular RRAMs, and wide bandgap semiconductors. From the first activity, he started to investigate Logic-in-Memory and neuromorphic architectures. The second interest led to TCAD simulation of GaN devices and to the development of safety-critical and energy-aware applications for automotive electronics. Paolo Pavan published more than 100 journal papers, 5 book chapters and 120 conference papers. Prof. Pavan was in Technical and Executive Committee of IEDM, Technical Committee of VLSI-TSA, IEEE-IRPS, ESSDERC and ESREF. He has been Technical Program Chair of ESSDERC 2014 and in the Steering Board of ESSDERC. He has been Guest Editor of the IEEE Transactions on Device and Material Reliability. He is an Associate Editor of IEEE Journal of Electron Device Society.

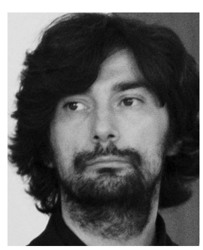

Simone Benatti (Member, IEEE) received a Ph.D. degree in electrical engineering and computer science from the University of Bologna, Bologna, Italy, in 2016. Currently, he has been appointed as an Assistant Professor at the University of Modena e Reggio Emilia. He has collaborated with several international research institutes and companies. Previously, he worked for eight years as an Electronic Designer and R&D Engineer of electromedical devices. In this field, he has authored or co-authored more than 90 papers in international peer-reviewed conferences and journals. His research interests include energy-efficient embedded wearable systems, signal processing, sensor fusion, and actuation systems. This includes hardware/software codesign to address performance, as well as advanced algorithms efficiently.